

# A Particle Simulation for the Axisymmetric Pulsar Magnetosphere: II. the case of dipole field

Tomohide Wada<sup>1\*</sup> & Shinpei Shibata<sup>2†</sup>

<sup>1</sup>*National Astronomical Observatory of Japan, Osawa 2-21-1, Mitaka, 181-8588, Japan*

<sup>2</sup>*Department of Physics, Yamagata University, Kojirakawa, Yamagata 990-8560, Japan*

Accepted 2011 July 26. Received 2011 July 25; in original form 2010 November 22

## ABSTRACT

The main issue of the pulsar magnetosphere is how the rotation power is converted into both particle beams which causes pulsed emissions, and a highly relativistic wind of electron-positron plasmas which forms surrounding nebulae shining in X-rays and TeV gamma-rays. As a sequel of the first paper (Wada & Shibata 2007), we carried out a three dimensional particle simulation for the axisymmetric global magnetosphere. We present the results of additional calculations, which are higher resolution model and higher pair creation rate cases, and a detailed analysis for the solution. We confined to demonstrate the cases of low pair creation rate, i.e., the magnetic field is fixed dipole. The radiation drag of the plasma is taken in a form with the curvature radius along the dipole magnetic field. The electrostatic interactions are calculated by a programmable special purpose computer, GRAPE-DR (Makino et al. 2007). Once pair creation is onset in the outer gaps, the both signed particles begin to drift across the closed magnetic field due to radiation drag, and they create outflow. Eventually, the steady magnetosphere has outer gaps, both signed outflow of plasma and a region in which the electric field is dominant extending from the equator. In the steady state, the magnetic field made by magnetospheric current is comparable to the dipole magnetic field outside of several light radii from the star. In much more pair creation rate model, the effect of modification of the magnetic field will bring about modification of the outflow of the plasma, requiring further study with higher pair creation rate model in a subsequent paper.

**Key words:** pulsars: general – magnetic fields – plasmas.

## 1 INTRODUCTION

Rotation powered pulsars are bright sources in the X-ray sky (e.g., Becker & Trümper 1997; Possenti et al. 2002; Kargaltsev & Pavlov 2008) and the gamma-ray sky (e.g., Nel et al. 1996; de Jager & Djannati-Ataï 2008) as well as in the radio (e.g., Hobbs et al. 2004), and they are identified as magnetized rotating neutron stars. The pulsed emissions originate in the accelerated particles in the magnetosphere. In addition, as a persistent source of high energy photons, we observe nebulae around young pulsars with synchrotron X-ray radiation (Kargaltsev & Pavlov 2008), inverse Compton TeV radiation (de Jager & Djannati-Ataï 2008), and thermal radiations from the neutron star (Becker & Trümper 1997). The emission from the nebula is caused by termination shock of the pulsar wind, which is believed to be relativistic outflow of magnetized pair plasmas carrying out most of the rotation power (Rees & Gunn 1974; Kennel & Coroniti 1984a,b). However, the nature of the pulsar wind and the radiation beam from the pulsar magnetosphere have remained a longstanding problem. As a primitive model, Goldreich & Julian 1969, hereafter GJ, suggested an axisymmetric steady model of pulsar magnetosphere in which the neutron star is assumed to be a perfect conductor surrounded everywhere by charge-separated force-free plasmas. The model anticipates that the plasma holds corotation with the star in the light cylinder although this corotational magnetosphere can be violated beyond

\* E-mail: tomohide.wada@nao.ac.jp

† E-mail: shibata@sci.kj.yamagata-u.ac.jp

the light cylinder. Then the GJ model assumes that the plasma is replaced by the acceleration along the opened magnetic field line beyond the light cylinder. On the basis of the copious plasma in the magnetosphere, the global relativistic magnetodynamics models are applied to help us understand acceleration of the pulsar wind (McKinney 2006a,b; Komissarov 2006; Bucciantini et al. 2006) and possible dissipation such as in magnetic neutral sheets may contribute to high energy pulsed radiation (Kirk et al. 2002). Against these studies, several studies showed that an aligned rotating neutron star should consist of the electrostatic charge clouds surrounded by the vacuum gaps without pulsar wind and therefore the steady solutions with outflow of the plasma are not self-consistent (See, Michel & Smith 2001). About the electrostatic solution, Krause-Polstorff & Michel (1985a,b, hereafter KM) performed a particle simulation for the axisymmetric model and showed formation of the gaps around the null surface with a rotating equatorial disc and polar domes. This model suggests a quiet electrosphere when the plasma is extracted only from the stellar surface, but the vacuum gap in the middle latitudes looked to be unstable against the pair creation cascade. Successively, Smith, Michel, & Thacker (2001) reconstructed the same result with a higher accuracy and even if the pair plasma were generated in the gaps at the middle latitudes, the quiet solution without pulsar wind was identified. In their models, the quiet solution is obtained that the particles are put at equilibrium positions along the dipole magnetic field line and this picture would be valid if the plasma is set down fully inside the light cylinder and the magnetic field is larger than the electric field. In other words, the effects of the inertia of the co-rotational plasma around the light cylinder is not considered. The same result is obtained by Pétri, Heyvaerts, & Bonazzola (2002b) who concluded a given total charge of the system determined by the net outgoing charged flux and the potential configuration is unfavorable for the particles to escape to infinity such as the active solution obtained by MHD approximation. However, the quiet solution should be modified to concern the leaking of the plasma at which the electrostatic plasma is in the vicinity of the light cylinder. As a possibility of radial outflow from the equatorial disc on the equator, Spitkovsky (2004) discovered the leaking mechanism of the equatorial disc caused by the diocotron instability with numerical simulation, which is also pointed out by Pétri et al. (2002a) with linear theory. The leaking of the disc should be significant to make the current in the vacuum region outside of the quiet electrosphere. But the time scale of the diffusion of the plasma in the vicinity of the light cylinder is much larger than the rotation period and therefore further study is needed to follow the global current structure with a much longer time scale such as a global numerical simulation with much more computational time with relativistic kinematics.

Contrary to the previous quiet solutions, we reported an active solution (Wada & Shibata 2007, hereafter, WS) with coexisting pulsar wind and outer gaps in which the effect of the inertia and radiation drag for the plasma is included by 3-dimensional particle simulation with special relativistic regime, and the simulation starts from the quiet solution as KM. Once pair plasmas are generated in the vacuum gaps around the quiet electrosphere, the positive charged outflow is formed near the equator and the negative charged outflow is formed from the polar region of the star. The outflow of plasma maintains the charge deficiency in the outer gaps. For the balancing of loss and the supply of particles from the outer gaps, the magnetosphere eventually settles in a steady state with pulsar wind. But there remains some problems to solve. At first, although our simulation showed that the wind coexists with the pair creating regions in the pulsar outer magnetosphere, the solution is only obtained by a lowest case of pair creation rate, where we carried out the simulation in which the current density around the star is less than the one of GJ model, and therefore magnetic field by the magneto-spheric current is negligibly-small in the light cylinder. If the pair creation rate taken to be large gradually in our simulation, the gaps tend to reduce and decrease the generation rate of the plasma and therefore the active structure might be disappeared. Although the drift motion of plasma caused by radiation drag force works as a leaking mechanism in closed magnetic field and is favorable to maintain the outer gaps, recalculation should be needed whether our active solution is maintained in higher pair creation rate models. Secondly, the obtained structure of the outer gaps contains some artifact due to the accuracy. The detailed flow pattern of plasma such as the poloidal current loop inside of the light cylinder was not clear because of low resolution of our previous work. We will simulate the lowest pair creation rate model again with higher resolution in which the unit charge of the particle is taken to be 1/10. At last, our particle simulation has numerical error, which is defined as the resolution of charge of simulation particle and the injection of the plasma from the inner boundary. In our previous work (WS), the polar potential drop is maintained in three times larger fraction than artifact level, present higher resolution model will decrease the error and could identify the existence. However the particle has large inertia length which is about 3% of the stellar radius and therefore we denote that our simulation could not resolve the size of polar cap accelerator.

Meanwhile the development of global magnetosphere, some phenomenological models which concerns the local structure for the magnetospheric activities have been developed: the polar cap models (Ruderman & Sutherland 1975; Arons & Scharlemann 1979; Zhang & Harding 2000; Harding & Muslimov 2002), the outer gap models (Holloway 1973; Cheng, Ho, & Ruderman 1986a,b; Romani 1996; Zhang & Cheng 1997; Hirotani & Shibata 1999; Takata, Shibata, Hirotani, & Chang 2006) and the slot gap model (Muslimov & Harding 2003, 2004) have been developed to explain the observed pulsed light curve and spectrum. The critical issue for these models is how the electric field along the magnetic field,  $E_{\parallel}$ , is maintained locally although the existence of the gap is implicit in these models. Although the adequacy of these gap models is achieved statistically by many further observations, but these models usually contain many degrees of freedom, for example, which are the surface magnetic field intensity of the pulsar, the inclination angle between magnetic axis and rotational axis, the viewing angle from the gaps and so on. Recently, the radiation from the pulsar magnetosphere with high-energy  $\gamma$ -ray bands has been observed

by the Fermi  $\gamma$ -ray telescope, and the 38 gamma-ray pulsars have been discovered (Abdo et al. 2009a,b, 2010), including 21 radio-loud and 17 radio-quiet. These observations could discriminate between the emission models located on the polar region or outer region, i.g., polar cap, slot gap, and outer gap. The Fermi telescope has also measured the spectral properties above 10 GeV with a better sensitivity than EGRET. It was found that the spectral shape of  $\gamma$ -ray emissions from the Vela pulsar is well fitted with a power law (photon index  $\Gamma \sim 1.5$ ) plus exponential cut-off ( $E_{\text{cut}} \sim 3$  GeV) model. The discovered exponential cut-off feature predicts that the emissions from the outer magnetosphere (Abdo et al. 2009c) are more favored than the polar cap region (Daugherty & Harding 1996), which predicts a super exponential cut-off with the magnetic pair-creation. Furthermore, the detection of the radiation above 25 GeV bands associated with the Crab pulsar has also predicted the high-energy emission in the outer magnetosphere (Aliu et al. 2008) with MAGIC (Major Atmospheric Gamma Imaging Cherenkov) telescope.

In this paper, we develop our global model such as linking the outer gap with the pulsar wind. In order to construct a solution, we utilize particle simulation in which particle motion and electric field are alternatively solved in the same way as the particle-in-cell (PIC) methods but with the magnetic field given with dipole in our present model. We simulate the generation of the plasma by pair creation in the gap and then obtain a steady state of the axisymmetric magnetosphere by solving the equation of motion including drag force due to curvature radiation and the electromagnetic fields. Since the motion of the individual particles is tracked, we can simulate any kind of drift motions for plasma, arising from the radiation drag force, the centrifugal force and the gradient of the magnetic field;  $\mathbf{f}_{\text{ext}} \times \mathbf{B}$  drift,  $\mathbf{E} \times \mathbf{B}$  drift and magnetic gradient drift. Here, we provide results of additional calculations and the detailed analysis for our steady solutions. We shall show that the trans-field drift by radiation drag plays an important role and eventually the electric field dominant region expanding to both sides of the equatorial plane makes a global poloidal current loop. But this paper considers cases of low rate of pair creation, and therefore modification of the original dipole field would be ignored as well as in our previous work. At first, the previous result (WS) of our steady solution was reconstructed with 10 times number of the particles and models with several pair creation rates were carried out. Our methods of calculations for the particle simulation are given in section 2, and the result is presented in section 3, and section 4 is for discussion.

## 2 NUMERICAL METHOD

### 2.1 Outline

We solve the motion of the particles and the electromagnetic field alternatively so as to obtain a self-consistent steady structure of the electromagnetic field and particle distribution. This method is similar to the well-established particle-in-cell (PIC) method. However, to obtain a steady solution, we use static solutions of the Maxwell equations, i.e., we omit the effects of time variation of the field ( $\partial \mathbf{E} / \partial t = \partial \mathbf{B} / \partial t = 0$ ). This enable us to use the programmable special purpose computer for astronomical N-body problem; GRAPE-DR (Makino et al. 2007), which calculates Coulomb interaction very rapidly with a high degree of precision at the position of the plasma.

In our simulation, generation of the particle is considered, which is not common in PIC methods. There are two cases: (1) electrons or protons on the stellar surface pop into the magnetosphere due to the unipolar induced electric field of the star, (2) electron-positron pairs are created due to photon-photon collision or magnetic pair creation in the magnetosphere. For the simplicity, the mass of both signed simulation particles is taken to be the same value, that is, the proton and positron are not distinguished, and the type of pair creation is not distinguished, that is, the detailed process of pair creation is not considered. We assume the pulsar to be a rotating spherical conductor in which magnetic field is uniform with the magnetized axis being parallel to the rotation axis. In this paper, because we consider the case of low rate of pair creation, which has much less current density than GJ model inside light cylinder, the modification of the dipole magnetic field near the star by the magneto-spheric current would be trivial. For this reason, the magnetic field outside of the star is assumed to be dipole, i.e.

$$\mathbf{B} = \frac{\mu}{r^3}(2 \cos \theta \mathbf{e}_r + \sin \theta \mathbf{e}_\theta), \quad (1)$$

where  $\theta$  is the colatitude,  $r$  is the distance from the center of the star,  $\mu = B_0 R^3 / 2$  is the dipole magnetic moment,  $B_0$  is magnetic field intensity at the poles,  $R$  is the stellar radius and  $\mathbf{e}_r$  and  $\mathbf{e}_\theta$  are the unit vector along  $r$  and  $\theta$  directions, respectively. These assumption gives the electric potential on the stellar surface,

$$\phi(\mathbf{R}) = \frac{\Omega \mu \sin^2 \theta}{cR} + \text{constant}, \quad (2)$$

where  $\Omega$  is the angular velocity of the star. This provides the inner boundary condition for the Poisson equation for the electric potential.

If the outside of the star is a vacuum, the electrostatic potential given by the solution of Laplace equation  $\nabla^2 \phi = 0$  is

$$\phi_v = \phi_1 + \phi_4, \quad (3)$$

where

$$\phi_1 = \frac{Q_{\text{sys}}}{r}, \quad (4)$$

$$\phi_4 = -\frac{\mu\Omega R^2}{3cr^3}(3\cos^2\theta - 1), \quad (5)$$

and  $Q_{\text{sys}} = \alpha 2\mu\Omega/(3c)$ , where  $\alpha$  is the non-dimensional net charge of the system. If we follow the Jackson's Gedanken experiment (Jackson 1976), we choose  $\alpha = 1$  as an initial condition, which corresponds to the +10 model for KM. Consequently, the vacuum electric field becomes

$$\mathbf{E}_v(\mathbf{r}) = -\nabla\phi_v = \mathbf{E}_4(\mathbf{r}) + \mathbf{E}_1(\mathbf{r}), \quad (6)$$

where

$$\mathbf{E}_4(\mathbf{r}) = -\frac{\mu\Omega R^2}{cr^4}(3\cos^2\theta - 1)\mathbf{e}_r - \frac{\mu\Omega R^2 \sin 2\theta}{cr^4}\mathbf{e}_\theta, \quad (7)$$

$$\mathbf{E}_1(\mathbf{r}) = \frac{Q_{\text{sys}}}{r^2}\mathbf{e}_r. \quad (8)$$

This vacuum solution has the surface charge density where

$$\sigma_v = \frac{\mu\Omega}{4\pi cR^2}(3 - 5\cos^2\theta) + \frac{Q_{\text{sys}}}{4\pi R^2}. \quad (9)$$

Given  $B_0$ ,  $R$  and the light speed  $c$ , all quantities in our simulation are normalized. In the following, the barred quantities indicate that they are normalized values. For example, electric charge is measured in units of  $B_0R^2$ , and  $\bar{Q}_{\text{sys}} = Q_{\text{sys}}/B_0R^2$ . In the following subsections, we describe the detailed method of our simulation.

## 2.2 Method of Solution for the Electric field

The space charge density in the magnetosphere is represented by limited number of simulation particles, i.e.,

$$\rho_m(\mathbf{r}) = \sum_{i=1}^n q_i \delta(\mathbf{r} - \mathbf{r}_i). \quad (10)$$

In simulation, we are concerned with the super particles which have the same mass and opposite signed charge with the same absolute value of the charge and therefore the difference in the mass of ion and that of positron is not considered. As we introduce later, the normalized value of the mass and charge for the super particle is represented by  $\bar{m}$  and  $\bar{q}$ , respectively. The electric potential in the magnetosphere is determined by Poisson's equation, i.e., the solution for electric potential is given by the superposition of the vacuum component (3) and space charge component, which is calculate by  $-\nabla^2\phi_m = \rho_m$ , with the boundary condition  $\phi_m(\mathbf{R}) = 0$ , and we have

$$\phi_m(\mathbf{r}) = \sum_{i=1}^n q_i \left[ \frac{1}{|\mathbf{r} - \mathbf{r}_i|} - \frac{R/r_i}{|\mathbf{r} - (R/r_i)^2\mathbf{r}_i|} - \left(1 - \frac{R}{r_i}\right) \frac{1}{r} \right] \quad (11)$$

for the electric potential,

$$\mathbf{E}_m(\mathbf{r}) = \sum_{i=1}^n q_i \left[ \frac{\mathbf{r} - \mathbf{r}_i}{|\mathbf{r} - \mathbf{r}_i|^3} - \frac{R}{r_i} \frac{\mathbf{r} - (R/r_i)^2\mathbf{r}_i}{|\mathbf{r} - (R/r_i)^2\mathbf{r}_i|^3} - \left(1 - \frac{R}{r_i}\right) \frac{\mathbf{r}}{r^3} \right] \quad (12)$$

for the electric field, and

$$\sigma_m = \sum_{i=1}^n q_i \left[ \frac{1}{4\pi R} \frac{R^2 - r_i^2}{|\mathbf{R} - \mathbf{r}_i|^3} - \frac{1}{4\pi R^2} \left(1 - \frac{R}{r_i}\right) \right], \quad (13)$$

for the surface charge density. Thus, the solution of the electric field with the boundary condition (2) is given in the forms,

$$\phi = \phi_m + \phi_v, \quad (14)$$

$$\mathbf{E} = \mathbf{E}_m + \mathbf{E}_v, \quad (15)$$

$$\sigma = \sigma_m + \sigma_v. \quad (16)$$

## 2.3 Popping of particles from the star surface

GJ pointed out that the rotation-induced electric field pulls charged particles from the stellar surface against the gravitational force. In the following, we describe how this process is realized in our simulation.

In vacuum conditions, the scalar product of the electric field and the magnetic field on the stellar surface is given by

$$\mathbf{E} \cdot \mathbf{B} = \frac{\Omega R B_0^2}{c} \cos\theta \left( \frac{\alpha}{3} - \cos^2\theta \right). \quad (17)$$

The sign of the electric field along the magnetic field ( $E_{\parallel}$ ) changes on the surfaces  $\cos\theta = \pm\sqrt{\alpha/3}$ , i.e., the negative charged

particles pop out from the polar region and positive charged particles pop out from the equatorial region. Once the charge is emitted from the stellar surface, they experience  $E_{\parallel}$  which changes sign on  $r = R + \sqrt{3}/\alpha \cos \theta$  for electron or on  $\theta = \pi/2$  for positron and ion (See, Jackson 1976). The electrons are emitted from the lower colatitude region are accelerated outward along the magnetic field line at first. For electron, after passing over the surface at which the minimum of the potential energy is given, the field aligned electric field decelerate the particles and they are reflected toward the stellar surface again. Then they accumulate near the surface and makes the polar dome of electrons because of the radiation drag force by the curvature radiation for the particle. At the same time, positrons or protons are emitted from the higher colatitudes accumulating on the latter surface, i.e., the equatorial plane, and making the equatorial positively-charged torus. Thus, the vacuum electric field tends to be screened out by the particles in the magnetosphere.

If the surface electric field along the magnetic field is shielded, the surface charge density becomes,

$$\sigma_{\text{GJ}} = \frac{3}{8\pi} \frac{B_0 \Omega R}{c} \sin^2 \theta. \quad (18)$$

This surface charge density is resulted in the kink of the magnetic field from the uniform one inside to dipole one outside under the ideal MHD condition. Although the surface charge density appearing on the stellar surface is  $\sigma$ , only the excess charge  $\sigma - \sigma_{\text{GJ}}$  is emitted from the stellar surface and therefore we expect that the surface charge density become  $\sigma_{\text{GJ}}$  in the steady condition. Thus, we replace  $\sigma - \sigma_{\text{GJ}}$  by the movable simulation particle. For simplicity, the work function of the particles on the stellar surface is not considered, that is the free emission of particles is assumed.

## 2.4 Parameter setting

In our simulation, we use the super particle with artificially-enlarged mass and charge of  $\bar{q} = 10^{-5}$ ,  $\bar{m} = 10^{-10}$  or  $\bar{q} = 10^{-6}$ ,  $\bar{m} = 10^{-11}$ . The number of particles representing the charge  $\rho_{\text{GJ,pole}} R^3$  is about  $10^4$  particles for  $\bar{q} = 10^{-5}$  model, which is same setting with WS, and  $10^5$  particles for  $\bar{q} = 10^{-6}$  model, respectively. Actual numbers of the particle is increased by pair creation, the total number of particles in the simulation domain jumps tenfold for them and therefore it needs heavy number of calculation related to square of the number of particle for Coulomb interaction in one step. Thus, we gain the privilege of using the GRAPE-DR, which is a programmable special purpose computer for Astronomical N-body problems, to calculate interaction between the particles.

In a realistic pulsar magnetosphere, the minimum scale of the motion of the plasma is gyro radius, which is  $r_g = 1.7 \times 10^{-2} r_3 \gamma \gamma_T$  cm for an electron or a positron, where  $\gamma$  is Lorentz factor of the particle  $r_3 = (r/R)^3$ , and  $\gamma_T = \gamma/10^7$  respectively. We use super particles with a larger mass-charge ratio than the real one. We take  $\bar{\Omega} = 0.2$  and  $\bar{m}/\bar{q} = 10^{-5}$ . For the definition of the numerical parameters, a typical gyro radius of the simulation particle on the pole is set to be  $10^{-5}$  stellar radius, and therefore the corresponding time step is set in  $d\bar{t} = 10^{-5}$ . Since the valid time step of particle for the gyro motion increases proportionately to the distance cubed from the star  $\sim \bar{r}^3$ , we use the individual time step for each simulation particle adapted to the position to reduce the total numbers of the integration time. As we introduce the size of numerical domain later, we have to follow these particles over several dynamical time length of the simulation domain until a steady condition is achieved. It takes about 6 rotation periods of the star, i.e.,  $\bar{t}_{\text{sim}} \sim 200$ .

For the unipolar induced electric potential by the rotational magnetized conductor, the available maximum energy of the particle is estimated by the open field line voltage

$$\phi_{\text{eff}} = \frac{\mu \Omega^2}{c^2} = 1.6 \times 10^{14} \left( \frac{P}{0.2 \text{ sec}} \right)^{-2} \text{ Volt}, \quad (19)$$

which gives maximum Lorentz factor of

$$\gamma_{\text{max}} = \frac{q \mu \Omega^2}{m c^4} = 3.2 \times 10^8 \left( \frac{P}{0.2 \text{ sec}} \right)^{-2} \quad (20)$$

for electron and positron. Note that if the Lorentz factor of a particle becomes  $\gamma_{\text{max}}$ , the gyro radius in the vicinity of light cylinder becomes the same order of the light radius. In other words, as expected, the localized acceleration region has much smaller potential drop than  $\phi_{\text{eff}}$ , the gyro radius of the particles is much smaller than the light radius. In our simulation, the gyro radius  $\bar{r}_g$  of all accelerated super particles is guaranteed smaller than the size of the light radius; typically  $\bar{r}_g = 10^{-2} \bar{R}_l$  for an accelerated particle corresponds to the Lorentz factor  $0.1 \gamma_{\text{max}}$  at the light radius.

## 2.5 Inner and Outer boundaries

For the injection of the particles from the stellar surface, the surface charge  $(\sigma - \sigma_{\text{GJ}}) \Delta S$  is replaced by the simulation particles, where  $\Delta S$  is the surface element of the stellar surface. If the particles are set on the stellar surface, they are pulled back by the mirror charge, i.e., the second term of (12). If this attractive field larger than the induced electric field, it prevents extraction of particles from the stellar surface as an artificial work function. Then the assumption of free emission of the particle from the stellar surface is not achieved. We put the particles above altitude of  $\bar{h}_c$  from the stellar surface to avoid this artificial

attractive force. We chose  $\bar{h}_c = 0.04$  for  $\bar{q} = 10^{-5}$  model,  $\bar{h}_c = 0.013$  for  $\bar{q} = 10^{-6}$  model, respectively. If the particles go back into the sphere with radius  $r = R + \bar{h}_c$ , the particles are deleted in the numerical region. It is notable that the numerical thin vacuum layer does not change the result at all.

To save the total number of simulation particles, we remove the particles beyond a sphere with the radius  $R_{\text{OB}}$  and the removed charge is reduced from  $Q_{\text{sys}}$ . The size of outer boundary is taken to be larger than the one of the accelerating region ( $\sim R_1$ ), that is, we chose  $R_{\text{OB}} = 10R_1$ . In our simulation, the removed particles beyond the outer boundary have positive total energy (kinetic plus potential), and we consider they would be outflow. To examine the effect of the size of the outer boundary, the larger outer boundary models, which are  $R_{\text{OB}} = 20R_1$ ,  $30R_1$  are investigated, then we confirmed that the structure of the magnetosphere inside the sphere with radius  $8R_1$  is not affected by the sizes of the outer boundaries. Thus, we use  $R_{\text{OB}} = 10R_1$  as our standard model.

## 2.6 Particle motion

The equation of motion of the particles is given by

$$m_i c \frac{d\gamma_i \boldsymbol{\beta}_i}{dt} = q_i [\mathbf{E}(\mathbf{r}_i) + \boldsymbol{\beta}_i \times \mathbf{B}(\mathbf{r}_i)] + \mathbf{f}_{\text{rad},i}, \quad (21)$$

where  $m_i$ ,  $q_i$ ,  $\mathbf{r}_i$  and  $\boldsymbol{\beta}_i$  are the mass, the charge, the position and the velocity of the  $i$ -th particle and  $\mathbf{f}_{\text{rad},i}$  indicates the drag force due to curvature radiation of the accelerated particles. In this paper, the magnetic field is not deformed by the magneto-spheric current. The radiation drag force of the particles is given

$$\mathbf{f}_{\text{rad},i} = -\frac{2}{3} \frac{q_i^2}{R_c^2} \gamma_i^4 \frac{\mathbf{p}_i}{|\mathbf{p}_i|}, \quad (22)$$

where  $R_c$  is the curvature radius along a dipole magnetic field line at the position of the particle. Substituting  $\varpi^2/r^3 = 1/r_{\text{eq}} = \text{const}$ , the curvature radius is given by

$$R_c = f \frac{r}{3 \sin \theta} \quad \text{with} \quad f = \frac{(4 - 3r/r_{\text{eq}})^{3/2}}{2 - r/r_{\text{eq}}}, \quad (23)$$

where  $r_{\text{eq}}$  is axial distance of the point at the intersection of dipole magnetic field line and the equatorial plane. Because  $1 < f < 4$  with  $0 < r/r_{\text{eq}} < 1$ , we take  $R_c = 4r/(3 \sin \theta)$  approximately.

If the Lorentz factor of the particle increases, (22) become comparable to the Lorentz force, and such particle has  $\mathbf{f}_{\text{rad}} \times \mathbf{B}$  drift motion crossing the dipole magnetic surface. The critical Lorentz factor for this effect is given by

$$\gamma_d = \left( \frac{3\pi\mu}{qcP} \right)^{1/4}. \quad (24)$$

For a realistic pulsar magnetosphere, it corresponds to  $\gamma_d = 3.6 \times 10^7 P_{0.2}^{-1/4} (R_c/R_1)^{1/2}$ . Considering the dependency of the distance for  $R_c$ ,  $R_c \sim R_1$  in the vicinity of the light cylinder. For electron,  $\gamma_d/\gamma_{\text{max}} = 0.11$  with  $P = 0.2$  sec and  $\mu = 10^{30}$  gauss  $\text{cm}^3$ , and thus the particles accelerated with 11% of the open field line voltage suffer from the such drift motion. On the other hand, for our simulation particles,  $\gamma_{d,\text{sim}}/\gamma_{\text{max},\text{sim}} = 0.0055$  for  $\bar{q} = 10^{-5}$  model and  $\gamma_{d,\text{sim}}/\gamma_{\text{max},\text{sim}} = 0.0098$  for  $\bar{q} = 10^{-6}$  model, respectively, i.e., once the kinetic energy of particles become 1% of  $q\phi_{\text{max}}$ , the radiation drag force is comparable to the Lorentz force. As a result, the radiation drag force for the super particle would be exaggerated. To perform radiation drag force properly, we introduce the reduction factor  $\eta$ , namely  $\gamma_i$  in (22) replaced by  $\eta\gamma_i$  and take  $\eta = 0.05$  for  $\bar{q} = 10^{-5}$  model and  $\eta = 0.089$  for  $\bar{q} = 10^{-6}$  model respectively although we simulate with  $\eta = 1$  in previous work.

## 2.7 A Test Run: Reproduction of quiet solution

The pair creation in the gap has a significant role in the structure of the magnetosphere. If pair creation is suppressed, the static magnetosphere by KM is reproduced. Following up to the Jackson's gedankenexperiment (Jackson 1976), our simulation starts with the condition that the positively charged magnetized rotating conductive sphere is initially put at the origin in a vacuum. The charge separated particles are emitted from the stellar surface and are accelerated by the induced electric field along the magnetic field lines. But the energy of the particles is lost due to the radiation drag force with time. The particles are located at the bottom of the potential along the magnetic field line, i.e. the force-free surfaces where the magnetic field aligned electric field vanishes. In vacuum, the force-free surfaces are polar domes and the equatorial plane. The inside of the polar force-free surfaces are filled with the negative charges emitted from the polar caps of the stellar surface, and they extend upward and form north and south force-free domes. Similarly, the positive particles accumulate above and below the equatorial plane and form a force-free torus. Eventually the field aligned electric field on the stellar surface is shielded, and the static negative charged domes above the poles and the static equatorial positive charged disc are formed. Fig. 1 shows the static particle distribution with the equipotentials  $\phi$ . For comparison, they are superposed on the co-rotational equipotentials which is given by  $\phi_{\text{co}} = \Omega\mu\psi/c$ , where  $\psi = \mu \sin^2 \theta/r$  is the dipole magnetic flux function. The equipotentials follow the co-rotational

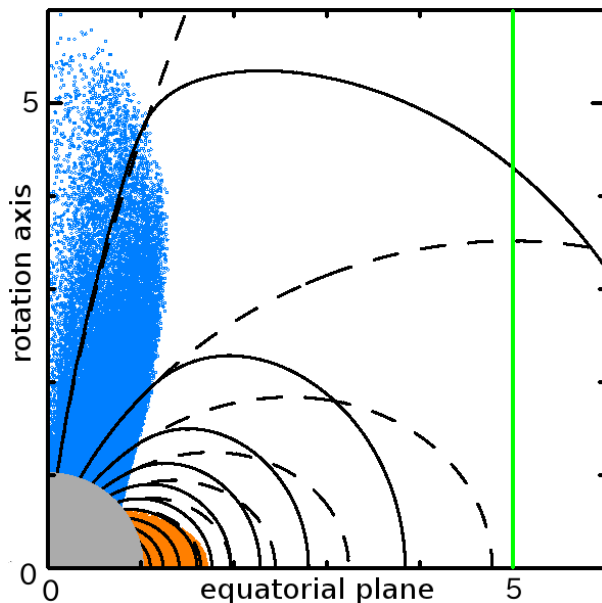


**Figure 1.** The particle distribution and the equipotentials for  $\alpha = 1$  and  $q_{\text{unit}} = 10^{-6}$  model. The orange and cyan points are positive and negative particles on the meridional plane  $(\varpi, z)$ , respectively. The light cylinder is located at  $\varpi = 5$  with the green line. The broken lines are the corotational equipotentials. The solid lines are the equipotentials. The contour level is taken with equal interval at  $0.5\phi_{\text{eff}}$ .

equipotentials in the negative charged clouds and the inner part of the positive charged torus close to the stellar surface. In the cusp of the torus, the two kinds of equipotentials are deviated but they are parallel. Roughly, the  $E_{\parallel}$  is screened out in the both signed charged clouds. Meanwhile, the electric field in the vacuum region faces the direction such that particles draw back to the cloud with the same sign, and therefore the cloud-vacuum boundaries are stable.

The force-free plasma in the cloud has toroidal velocity by  $\mathbf{E} \times \mathbf{B}$  drift, which is given by

$$v_t = \varpi\Omega + c\varpi \frac{d\phi_{\text{nco}}}{d\psi}. \quad (25)$$

where  $\varpi$  is the radius in the cylindrical coordinates and  $\phi_{\text{nco}} \equiv \phi - \phi_{\text{co}}$ . The coincidence of  $\phi$  and  $\phi_{\text{co}}$  in the cloud means  $d\phi_{\text{nco}}/d\psi = 0$ , i.e., the co-rotational motion of the plasma. The value of the potentials fall off faster than the co-rotational one in the outer part of the disc, and therefore the term  $c\varpi d\phi_{\text{nco}}/d\psi$  gives super-rotation in the (25). In this structure, the toroidal velocity of the plasma in the outer part of the disc was less than light speed because of the size of the disc is much less than the light cylinder.

As mentioned in subsection 2.5, note that our simulation has artificial thin vacuum layer between the inner boundary and the stellar surface. The region causes deviation of the toroidal velocity from corotation in the polar dome. Fig. 2 shows  $d\phi/d\psi$  for the  $10^{-5}$  model and the  $10^{-6}$  model in unit of  $\Omega/c$  on the inner boundary. This curve has a symmetry on both sides of the equator. Most of the cloud co-rotates except for near the poles and the equator. The maximum deviation from the co-rotational velocity is 40% for the  $10^{-5}$  model and 30% for the  $10^{-6}$  model, respectively. Although the error is large on the equatorial plane, an affect near the equator is trivial because the co-rotational velocity is originally small at this place. But the deviation by the numerical error near the pole is significant if polar electric domes expand in the vicinity of the light cylinder. In our simulation, the polar force-free electric dome, which connects to the stellar surface along the magnetic field anchored at 3 deg for  $10^{-5}$  model and 1 deg for  $10^{-6}$  model, has about 10% sub-rotational velocity from the light speed with the distance of light radius.

## 2.8 The treatment of pair creation and initial condition

Fig. 3 shows the distribution for strength of the electric field along the magnetic field line ( $E_{\parallel}$ ) on the meridional plane for the static solution. A strong intensity region is appeared in the middle latitudes, while the less intensity is appeared in the charge clouds. For the static solution, there is a vacuum gap in the middle latitude with a potential drop of  $\sim 2\phi_{\text{eff}}$ . In the vacuum gap, the maximum intensity of  $E_{\parallel}$  is typically  $E_{\parallel, \text{max}} \sim 3B_1$  at  $(\varpi, z) = (1.8R, 1.4R)$  on meridional plane, where  $B_1 \equiv \mu/R_1^3$  is the dipole magnetic field intensity at the light radius on the equator. If the charge particles are injected into the gap, they will be immediately accelerated to ultra-relativistic regime by the  $E_{\parallel}$ , and radiate the  $\gamma$ -rays by the curvature

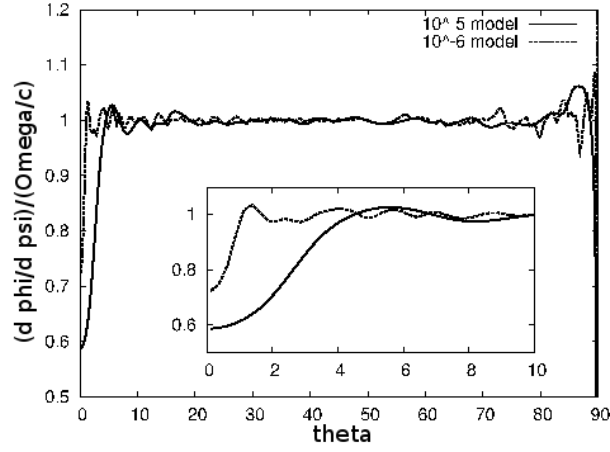


**Figure 2.**  $d\phi/d\psi$  normalized by  $\Omega/c$  versus the colatitude on the inner boundary. The small panel is close up near the polar region from 0 deg to 10 deg.

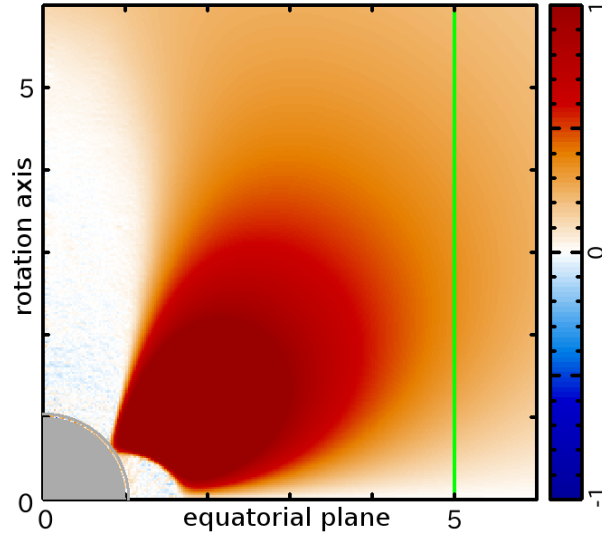


**Figure 3.** The  $E_{\parallel}$  intensity map for the pair starved static structure with  $\bar{q} = 10^{-6}$  model on the meridional plane, where the color intensity is normalized by  $B_1$ . The light cylinder locates at  $\varpi = 5$  with green line.

radiation process, whose power is given by

$$\dot{\epsilon}_c = \frac{2q^2\gamma}{3R_c^2}. \quad (26)$$

The typical Lorentz factor of the accelerated particles is estimated by the force balance between the radiation drag force and the electric force, i.e.,  $qE_{\parallel} = \dot{\epsilon}_c/c$ , which gives

$$\gamma_{\text{sat}} = \left( \frac{3\mu R_c^2}{2qR_1^3} \right)^{1/4}. \quad (27)$$

Then, the typical energy of the emitted  $\gamma$ -rays is given by

$$\epsilon_{\gamma} = \frac{3hc\gamma_{\text{sat}}^3}{4\pi R_c}. \quad (28)$$

With typical parameters of the pulsars, we obtain the Lorentz factor of  $\gamma_{\text{sat}} = 1.1 \times 10^6 P_{0.2}^{1/2} (R_c/R_1)^{1/2} (E_{\parallel}/B_1)^{1/4}$  and the photon energy of  $\epsilon_{\gamma} = 1.4 \times P_{0.2}^{3/2} (R_c/R_1)^{1/2} (E_{\parallel}/B_1)^{3/4}$  GeV. In the present work, we simplify the pair-creation process, that is, (1) we do not distinguish between the photon-photon pair-creation process and the magnetic pair-creation process, and (2) we ignore the effects of the collision angle between the  $\gamma$ -rays and soft-photons (or the magnetic field). In our simulation, we determine the pair-creation position using the condition that  $\epsilon_{\gamma} > 2mc^2$ , implying the pair-creation is occurred at the position, where the electric field is stronger than  $E_{\text{cr}} = 6.6 \times 10^{-5} P_{0.2}^2 (R_c/R_1)^{2/3} B_1$ .  $\epsilon_{\gamma} > 2mc^2$  is not applicable in reality because of the effect of collision angle of the two photons. On the other hand, we shall see below that actual setting of the

| name | $\bar{q}$ | $\bar{E}_{\text{cr}}$ | $\tau_{\text{pr}}$ | $\Delta r$ | $\Delta\theta$ |
|------|-----------|-----------------------|--------------------|------------|----------------|
| A0   | $10^{-5}$ | $10^{-3}$             | 2.0                | 0.1        | $2^\circ$      |
| A1   | $10^{-5}$ | $10^{-3}$             | 1.0                | 0.1        | $2^\circ$      |
| A2   | $10^{-5}$ | $10^{-3}$             | 0.2                | 0.1        | $2^\circ$      |
| A3   | $10^{-5}$ | $10^{-3}$             | 0.1                | 0.1        | $2^\circ$      |
| A4   | $10^{-5}$ | $5 \times 10^{-4}$    | 2.0                | 0.1        | $2^\circ$      |
| A5   | $10^{-5}$ | $2.5 \times 10^{-4}$  | 2.0                | 0.1        | $2^\circ$      |
| B0   | $10^{-6}$ | $10^{-3}$             | 0.2                | 0.1        | $1^\circ$      |

**Table 1.** The numerical parameter of simulation.

value of  $E_{\text{cr}}$  is much larger than this value in the numerical simulation since the accuracy of the electric field is much larger than  $E_{\text{cr}}$ .

For our simulation, the pair creation is performed in the following way. We introduce the critical electric field intensity to generate pairs in the simulation as parameters, that is  $\bar{E}_{\text{cr}}/B_1 = 0.25, 0.125, 0.0625$  although they are larger than the realistic value. At first, the equally-spaced grid points  $(\bar{r}_i, \theta_j)$  are prepared with spherical coordinates in the meridional plane, where  $\Delta\bar{r} = 0.1$ ,  $\Delta\theta = 2^\circ$  for  $\bar{q} = 10^{-5}$  model and  $\Delta\bar{r} = 0.1$ ,  $\Delta\theta = 1^\circ$  for  $\bar{q} = 10^{-6}$  model, respectively. If the field-aligned electric field at a grid points  $\bar{E}_{\parallel}(i, j)$  is larger than  $\bar{E}_{\text{cr}}$ , then we put on  $n_{\pm} = n_{\text{M}}$  pairs around the grid, where  $n_{\text{M}}$  is multiplicity of the pair creation. The generation of pairs is repeated in every  $\bar{\tau}_{\text{pr}}$ , where we take  $\bar{\tau}_{\text{pr}} = 2.0, 1.0, 0.2$ , which are less than the light crossing time of the light radius. We consider  $n_{\text{M}}$  as a constant parameter and the lowest cases  $n_{\text{M}} = 1$  are carried out to guarantee the pure dipole magnetic field assumption. We set up the static solution as an initial condition of the simulation with pair creation effect, e.g., 3000 pairs are generated in the gaps with  $\bar{q} = 10^{-5}$  model with  $n_{\text{M}} = 1$  in initial. Table 1 provides the numerical set of parameters of simulation.

Note that the perturbation of a simulation particle makes error electric field. The maximum error of electric field caused by a simulation particle is roughly given by  $E_{\text{err}} = \bar{q}/\Delta^2$ , which is  $0.25B_1$  for  $10^{-5}$  model and  $0.025B_1$  for  $10^{-6}$  model in the present parameter setting, where  $\Delta$  is typical interval of the grid to estimate  $E_{\parallel}$  and we choose  $\Delta = 0.1R$ . If  $E_{\text{cr}}$  is taken to be much smaller than  $E_{\text{err}}$ , the pair is generated excessively and therefore the calculation is immediately broken by running out of the limit of the number of particles in our simulation.

### 3 RESULT

#### 3.1 Quiet Solution: without pair creation

As has been shown, if pair creation is suppressed, the electrosphere is composed of electronic domes above the pole, a positronic or ionic equatorial disc and vacuum gaps in the middle latitudes. It takes about one rotation period until the quiet state is achieved with  $\alpha = 1$ . We also simulate for smaller system charges of  $\alpha = 0.75, 0.5, 0.4, 0.3$  with  $\bar{q} = 10^{-6}$  model. The smaller the net charge, the larger the extent of the polar dome (see left panel of Fig. 4). This tendency has been stated by Krause-Polstorff & Michel (1985b) +10 and +4 models which correspond to our  $\alpha = 1$  and 0.4 models, respectively.

The same structures are identified as well as KM with  $\alpha \geq 0.4$  in our simulation because the polar dome falls in the light cylinder and therefore it satisfies the condition of rigid constraint for the particle by the dipole magnetic field. But the model with  $\alpha = 0.3$ , the static structure is changed. The global flow pattern of the particles for the model with  $\alpha = 0.3$  is shown in the right panel of Fig. 4. When we choose a model with  $\alpha < 0.4$ , the polar dome extends beyond the light cylinder and the azimuthal velocity of the particle in the dome increases with the axial distance although the azimuthal velocity is slightly small from the corotational velocity. Thus, the Lorentz factor increases close to  $\gamma_{\text{d}}$  near the light cylinder and then the radiation drag force of the particle makes  $\mathbf{f}_{\text{rad}} \times \mathbf{B}$  drift just out side of the light cylinder. Thus, the particles emitted along the polar magnetic field line migrate into the inner magnetic surface if they pass through the light cylinder, and they returns star just higher colatitude of their departure point. As a result, there are outflows of the negative particle from the polar region, which are bounded the magnetic surface footed on the stellar surface with 4.5 degree. Note that, for our case, the whole charge cloud is still in magnetic field dominant region ( $B > E$ ). When the outflows go beyond the light cylinder, they move across the inner magnetic surface by the  $\mathbf{f}_{\text{rad}} \times \mathbf{B}$  drift and they become inflow by the quadropole electric field in the vacuum region at the middle latitudes. Thus, the closed poloidal current loops above the pole are formed in several light radius. This is more favorable rather than the faraway loop of the electron made by attraction of the monopole electric field of the star suggested by Jackson (1976). Our result confirmed the same flow pattern of electrons given by Rylov (1977). Although a part of the edge of the dome has fast azimuthal velocity, the current density of the dome in the vicinity of the light cylinder is typically  $10^{-5} \rho_{\text{GJ,pole}c}$ , and therefore the modification of the dipole magnetic field should be ignored.

Fig. 5 shows  $\phi$  along two radial directions with  $\theta = 30^\circ$  and  $\theta = 90^\circ$  (equatorial plane), respectively. The former radial line passes through the polar dome, while the latter does through the equatorial disc. It is notable that the derivative  $d\phi/d\psi$

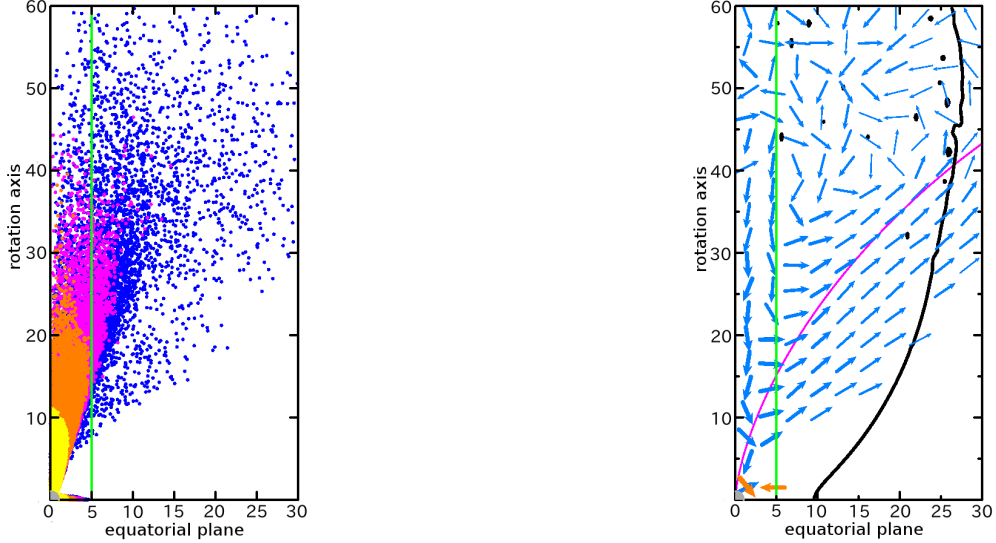


**Figure 4.** Left panel: The distributions of the particles on the meridional plane with simulated  $Q_{\text{sys}}$ 's, Colored dots indicate  $\alpha = 0.75, 0.5, 0.4, 0.3$  with blue, magenta, orange and yellow respectively. The light radius is located at  $\varpi = 5$  with green line. Right panel: the current density pattern on meridional plane for  $\alpha = 0.3$  model. The arrows indicate the direction of the current density of negative charged particle (blue) and positive charged particle (red). The magenta curve indicates magnetic field line footed on the surface with colatitude 4.5 degree. The boundary surface with  $E = B$  is drawn by solid curve.

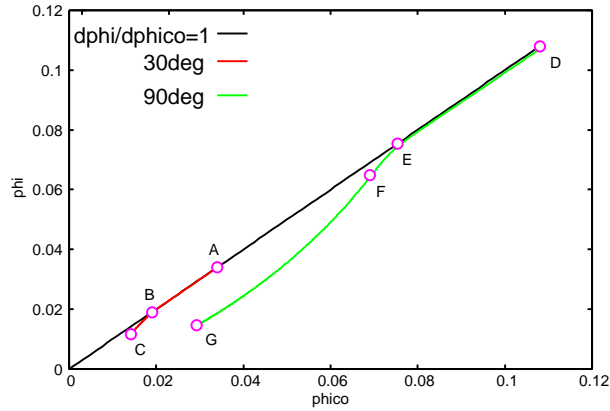


**Figure 5.** The electrostatic potential  $\phi$  along the radial line with  $\theta = 30^\circ$  (A-B-C) and with  $\theta = 90^\circ$  (on the equatorial plane) (D-E-F-G) as a function of the magnetic stream function  $\psi$ . The solid line indicate the co-rotational potential  $\phi_{\text{co}}$ .

indicates the angular velocity of the clouds. Along the line with  $\theta = 30^\circ$ , the electric potential  $\phi(\psi)$  follows the co-rotational  $\phi_{\text{co}}$  in between A and B in the figure, which correspond to the stellar surface and the surface of the cloud (cloud-vacuum boundary). This indicates that the cloud co-rotates with the star in the cloud. Along the line with  $\theta = 90^\circ$  (equator), the inner part of the disc between D and E follows the co-rotational  $\phi_{\text{co}}$ , and therefore they show co-rotation and  $E_{\parallel} = 0$ . The point F corresponds to the top of the equatorial disc. Because of  $d\phi/d\psi > \Omega/c$  in between E and F, the positive charge at the edge of the disc are in super-rotation. This part is connected to the vacuum gaps in the middle latitudes along the magnetic field line. The electric potential in the outer part of the disc decreases faster than the co-rotational potential. Thus, the super rotation of the disc top is obtained. Outside of the clouds (between B and C) is in vacuum, and  $\phi$  deviates from  $\phi_{\text{co}}$ , i.e.,  $E_{\parallel}$  exists. These features can actually be seen with the velocity of the particle in Fig. 6, i.e., one can see the co-rotational motion in the polar domes and in the inner part of the disc, the super-rotation in the outer part of the disc. The azimuthal velocities are not close to the light speed at the top of the equatorial disc, and therefore the radial diffusion mechanism by rotational inertia and radiation drag are negligible in such cases. Outside of the disc (between F and G) is in vacuum.

### 3.2 Active Solution: with pair creation

The steady solutions are obtained in about 4 rotation periods. For comprehending the trajectories of the particle, we have to know the magnitude relation between electric field and magnetic field and the effect of the drift motion caused by radiation

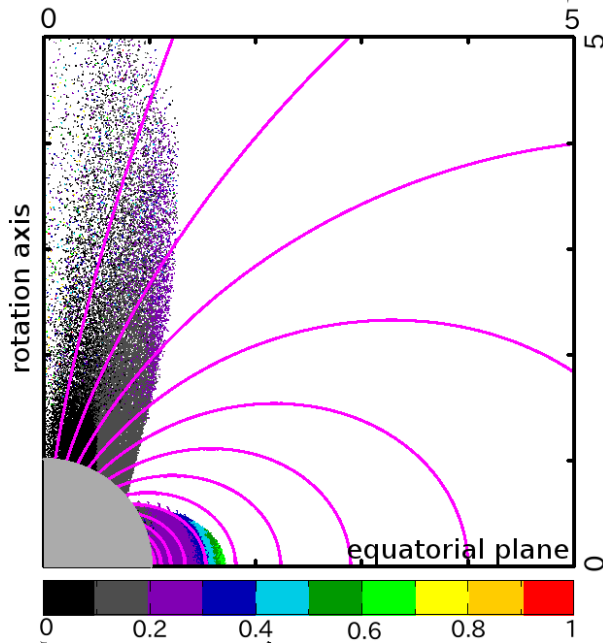


**Figure 6.** The particles color-coded with toroidal velocity on the meridional plane. The meaning of the colors is shown in the color bar just below the equatorial plane, where each color indicates the co-rotation speed at each axial distance. The solid curves are dipole magnetic field lines.

drag force. When the plasma is in the magnetic field dominant region (MDR), it tends to move along magnetic surface. However, once it is in the electric field dominant region (EDR), particles are accelerated toward the direction of the electric field. If  $E_{\perp} \sim B$  in MDR, the velocity of the  $\mathbf{E} \times \mathbf{B}$  drift of the plasma is close to light speed. Then the radiation drag force for the particle is comparable to the Lorentz force, that is the Lorentz factor of the plasma becomes  $\gamma_d$ , which is given by (28). Such plasma drifts perpendicular to the magnetic surface by the  $\mathbf{f}_{\text{rad}} \times \mathbf{B}$  drift. It is notable that the  $\mathbf{f}_{\text{rad}} \times \mathbf{B}$  drift is opposite direction depending the sign of the charge, i.e., the positive charged particle drifts outward and the negative charged particle drifts inward.

In the left panel of Fig. 7, the typical trajectories of particle on the meridional plane are drawn with red and blue curves and EDR and MDR are bounded with thick curves. The EDR appears around the equatorial plane in a wedge-like shape beyond  $\varpi \sim 4.5 = 0.9R_l$  with the opening angle of about  $50^\circ$  from the equatorial plane. Although the EDR appears due to the monopole electric field in the quiet model (Jackson 1976; Rylov 1977), our present model has almost no net charge. The EDR seemed to have been formed by the global structure of the charge cloud, and in particular it would be due to the growing equatorial positive charged disc. The similar shape of EDR is discussed in the force-free model around Y-point by Uzdensky (2003). The angle between the EDR and the equatorial plane in our result is just wider than Their EDR. It is interesting that the structure of EDR is very similar although our result precludes the force-free approximation and assumes the magnetic field to be dipole elsewhere. In the right panel of Fig. 7, the luminous color-coded particle have the Lorentz factor being comparable with  $\gamma_d$ , i.e., the radiation drag force for the particle is comparable to the Lorentz force  $qB_1$ . They are mainly in the vicinity of the light cylinder. The positive charged particle near the equatorial plane just inside the light cylinder has the Lorentz factor with  $\gamma_d$ . At the same time, the negative charged particle in the vicinity of the light cylinder with the height above  $10R$ . The dusk color-coded dots in the right panel of Fig. 7 indicates the non-accelerated particles, i.e., they are co-rotating equatorial disc and conically-shaped polar domes. The background color of the left panel of Fig. 7 indicate the intensity of  $E_{\parallel}$ , which are color-coded red ( $E_{\parallel} > 0$ ), blue ( $E_{\parallel} < 0$ ) and white ( $E_{\parallel} = 0$ ), respectively. Both sides of the outer gap, the  $E_{\parallel}$  is shielded and there is the co-rotating charged clouds.

In the left panel of Fig. 7, the flow of the positive particle generated in the outer gap goes into EDR, it easily goes out beyond the light cylinder ( $a_0 \rightarrow a_1$ ). The plasma at the outer edge of the disc at  $b_0$  has a fast azimuthal velocity, and therefore they are slipped out by  $\mathbf{f}_{\text{rad}} \times \mathbf{B}$  drift ( $b_0 \rightarrow b_1$ ). Meanwhile the flow of the negative particles generated in the outer gaps moves back to the star ( $c_0 \rightarrow c_1$ ) with colatitude  $24^\circ < \theta < 34^\circ$  on the stellar surface, and re-emitted from the polar region. The polar flow is separated by the magnetic surface footed on the stellar surface with colatitude  $10^\circ$ , where the equipotential surface of  $\phi = 0$  connects up to the star. For the lower colatitude region, it is outflow drawn by  $d_0 \rightarrow d_1$ . For the other region, it is circulation on the meridional plane, which is starting from the polar annulus with the colatitude  $10^\circ < \theta < 12^\circ$ , and returning to the annulus with colatitude  $18^\circ < \theta < 24^\circ$  ( $e_0 \rightarrow e_1 \rightarrow e_2 \rightarrow e_3 \rightarrow e_4$ ). On the way through  $e_0 \rightarrow e_1$ , the flow having fast azimuthal velocity migrates to the inner magnetic surface because of  $\mathbf{f}_{\text{rad}} \times \mathbf{B}$  drift. Once it moves in EDR, it is

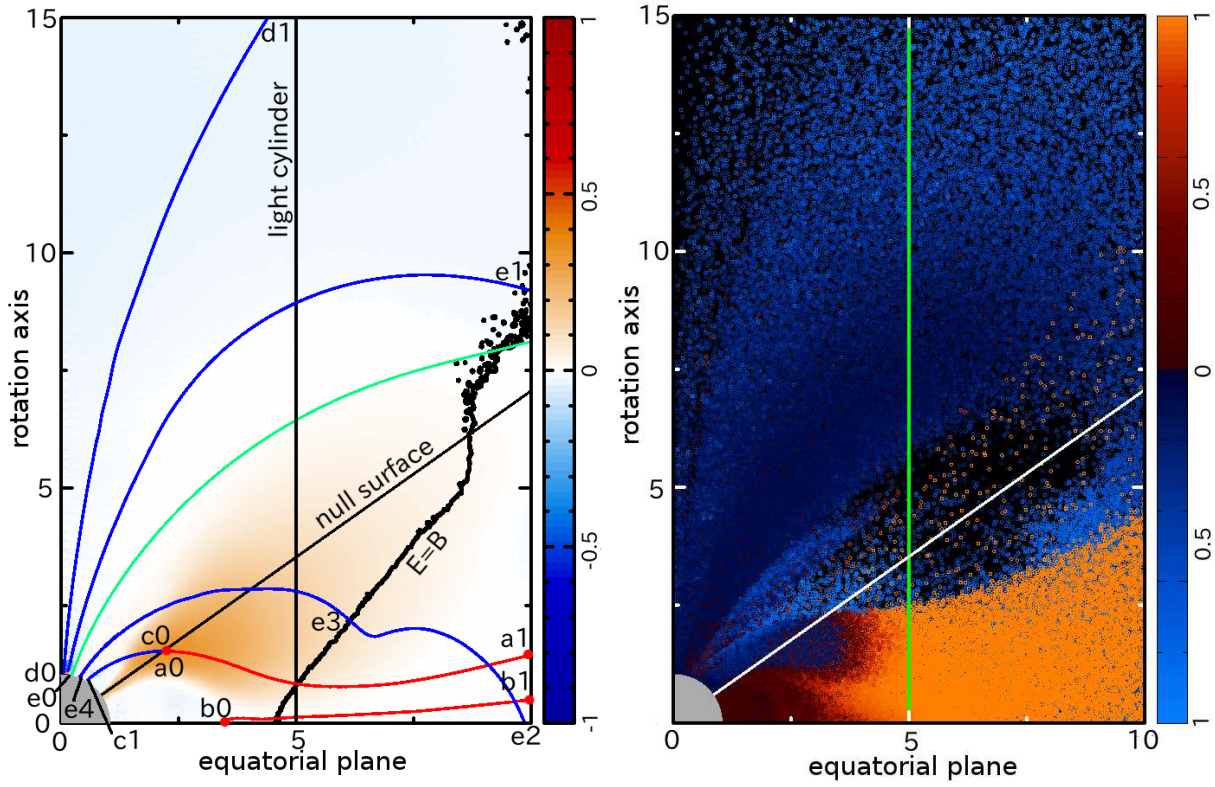


**Figure 7.** Left panel: typical trajectories of the particle and  $E_{\parallel}$  intensity map, the curves are color-coded with blue (for the negative charged particle), red (for the positive charged particle) and the color map indicates electric field intensity normalized by  $B_1$ . The thick solid curve indicates isosurface with  $E = B$ , and the solid curve with green means equipotential surface with  $\phi = 0$ . Right panel: Lorentz factor of the particles, which are color-coded with the Lorentz factor normalized by  $\gamma_d$ . For both panels, the light cylinder is located at  $\varpi = 5$  and the line in the middle latitude is null surface. )

accelerated and passes over the equatorial plane. Because of the plane-symmetric fashion about the equatorial plane, the flow having the same trajectory in the opposite hemisphere returns from  $e_2$ , then it moves in MDR ( $e_2 \rightarrow e_3$ ). Thus, it returns along a magnetic field line just outside the pair creating region in the middle latitude ( $e_3 \rightarrow e_4$ ).

The overhead view of the steady solution is shown in Fig. 8. The intensity ratio of the dipole magnetic field and the magnetic field made of the magnetospheric current in the steady state is drawn with gray scale map. The current density normalized by  $\Omega B / (2\pi)$  on the meridian plane is drawn with color-coded arrows and the electrostatic equipotentials normalized by the  $\phi_{\text{eff}}$  are drawn with the curves. The green curves indicates that the value of the equipotential is zero. The value of the potential is negative in the lower colatitude region and is positive in the higher colatitude region. The contour level is incremented by  $-3, -2, -1, 0$  with common logarithm from the zero-equipotential surface for both signs of potentials. It shows the assumption of dipole magnetic field is valid in the light cylinder and especially round about the equatorial plane, although the magnetic field made by the magnetospheric current is comparable to the dipole field in the middle latitude about beyond  $3R_1$ , where magnetic flux is modified to be opened. The circulation pattern of the flow in the present result would turn down if the modification of the magnetic field is concerned. The magnetic field made of the magnetospheric current is trivial inside the light cylinder, namely the structure of the outer gaps and pair creation rate should not be affected in present model if the modification of the dipole magnetic field is considered. In contrast, outside of several light radius, the magnetic field made of the magnetospheric current is comparable to the dipole magnetic field. However, there are almost in EDR, and therefore the particle flow is controlled by the electric field. Concerning the global structure of the current and equipotential surfaces, the negative charged flowed out in a lower latitude and the positive charged flowed out in a higher latitude. However, the system of the charge of our result is almost neutral, that is the monopole electric field would not prevent reversed sign outflow at a great distance. Eventually both outflows have enough kinetic energy larger than the potential energy at the outer boundary, and therefore they can reach infinity beyond the outer boundary. Inside of the sphere about with radius  $3R_1$ , there are poloidal current loops caused by  $\mathbf{f}_{\text{rad}} \times \mathbf{B}$  drift from equatorial plane to the pole, which mainly consist of negative charged flow. In previous paper, the parameter of the radiation drag force,  $\eta$  is taken to be unit so that the circulation of the both signed charge caused by the  $\mathbf{f}_{\text{rad}} \times \mathbf{B}$  drift is incident. In present result, there are few returning positive charges although the poloidal current structure is similar to that in previous work.

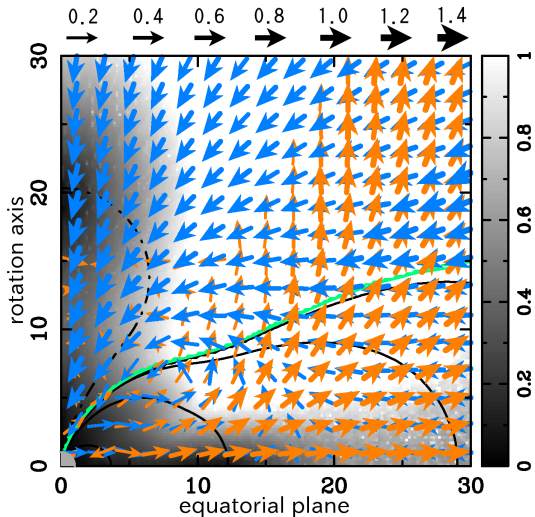


**Figure 8.** The arrows indicate the current density made of positive charge (orange) and negative charge (cyan), which are normalized by  $\Omega B/(2\pi)$ . The intensity ratio of dipole magnetic field and the magnetic field made of the magnetospheric current is drawn by gray scale color-coded map, that is  $|B_q|/|B_d|$ . The curves are electrostatic equipotentials normalized by  $\phi_{\max}$  with common logarithm, where  $\phi = 0$  is colored with green, the solid curves indicates  $\phi > 0$  and the dashed curve indicates  $\phi < 0$ .

## 4 DISCUSSION

### 4.1 Comparison with the quiet solution

Smith, Michel, & Thacker (2001) concluded that their result for the axisymmetric magnetosphere is quiet because the pair plasma which moves along the dipole magnetic field lines screens out the  $E_{\parallel}$  in the outer gaps and therefore the pair creation is stopped. They implied that activity of pulsar is essentially caused by obliqueness (see also Michel 2004). Although the similar screening of the outer gaps is shown in our simulation, but intensity of the electric field is maintained to generate pair plasma. We note that our active solution arise from taking smaller threshold intensity of electric field for pair creation than Smith, Michel, & Thacker (2001) and solving the equation of motion for each particle without the assumption of restraint of plasma along the dipole magnetic field line. As a result, we showed that if the radiation drag of the particle and the supply of the pair plasma in the gaps are performed, the quiet system should be broken and migrates over to the active system with gaps and both signed outflows of the plasmas nevertheless the rate of the pair creation is taken to be small as the modification of the dipole magnetic field is omitted. Some fraction of the positive charge generated in the outer gaps accumulates the equatorial plane, and therefore the super rotating disc is growing and the azimuthal velocity increases, and then the Lorentz factor increases as the light cylinder reaches in some fraction of  $\gamma_d$ . The particles at the cusp of the disc start to leak out due to the  $\mathbf{f}_{\text{rad}} \times \mathbf{B}$  drift. If the potential drop in the outer gap is  $f$  in fraction of the effective voltage, the trans-field drift would take place beyond  $(1-f)R_l$ , i.e., it is likely that radiation drag causes trans-field drift motion within the light cylinder. As has been shown, this effect creates an outflow of positive charged particles even if the dipole magnetic field is closed, and it is favorable to keep the outer gaps.

As diocotron instability of differential rotation disc is pointed by Spitkovsky (2004); Pétri, Heyvaerts, & Bonazzola (2002a); Pétri (2007), the leaking of the edge of disc is realized after several rotation periods for our simulation. Although it prompts decrease of the charge from the system even if all particles are trapped in closed magnetic surface or pair creation is suppressed, but the speed of the growth of the disc decreases when the disc grows in vicinity of the light cylinders and the decrease of charge is trivial compared with total charge of the disc. We simulated to confirm how the diocotron instability affects the global structure of the disc over 20 rotation periods for the pair starved electrosphere, which is barely acceptable to carry out for our present environment. At least we realized that the diffusion by the diocotron instability was not so significant in such a time scale, although the diffusion by  $\mathbf{f}_{\text{rad}} \times \mathbf{B}$  changes the quiet electrosphere in several rotation periods. Note that the growth of the disc is made by the pair created positive charges in the outer gaps and the main component of leaking of the disc is made by  $\mathbf{f}_{\text{rad}} \times \mathbf{B}$  drift of the particle in our simulation and even the loss of the positive charge from the edge of the disc is much lower than the outflow from the outer gaps to EDR (See, left panel of Fig. 7,  $a_0 \rightarrow a_1$ ).

If copious plasma is supplied to the equatorial disc from the outer gaps, another important issue remains the region, the so-called Y-point, is expected to have the electric field larger than the magnetic field in the force free theory (Uzdensky 2003). In the next paper, we treat higher rates of pair creation, for which modification of the magnetic field becomes significant in the vicinity of the light cylinder. Then, some poloidal magnetic flux is opened and toroidal magnetic field would be anti-parallel on both sides of the equatorial plane in which the dissipation of the magnetic field is expected to accelerate the particles by

dissipation process of the magnetic field. Thus, trans-field leakage of the particle around the Y-point is a very interesting issue, but we postpone further discussions until the simulations with higher rates of pair creation are performed.

## 4.2 Formation process of steady solution

Although the steady solution is stated in section 3.2, here we discuss by the stage of the active solution. Once pair creation is on set, the pair plasmas are generated at first in middle latitudes in which  $E_{\parallel}$  is stronger than  $E_{cr}$  (see Fig. 3). The pairs created in the outer gaps are immediately separated in opposite directions along a magnetic field line by  $E_{\parallel}$ . Then, most of the positive charges move into EDR to form an outflow. At the same time, the negative charges move inward. They returns to the star and are re-emitted from the polar regions so that the height of the dome increases. The outflow of the positive particles causes significant change to the global structure: the system charge, which is initially assumed to be positive, is reduced. As a result, the potential of the polar region becomes negative, and a part with lower latitude of the polar domes becomes outflow. The other half of the polar dome grows and crosses over the light cylinder. The Lorentz factor of the plasma increases to bring about trans-field motion by radiation drag force. It is notable that the negative charges obtain kinetic energy if they drift toward inner magnetic surfaces. Some part of the particles become outflow if the kinetic energy is larger than the potential energy at the outer boundary, and therefore the separatrix of the negative charged flow is made on the equator with  $3R_1$  in present result although it is set on the equator about with  $8R_1$  in previous work. The difference might be made by the resolution of the charge and the detailed mechanism of the formation of the separatrix with modification of magnetic field needs additional simulation in future work. Thus, steady state is found in equal losses of both particle species and the lost particles are supplied by the outer gaps.

In our simulation, we demonstrate the generation of the particles intermittently in some periods  $\bar{\tau}_{pr} = 0.1, 0.2, 1.0, 2.0$  for the pair creation and a fixed period  $\bar{\tau}_{po} = 0.1$  for the popping from the stellar surface. All steady results had the same geometry of the charge clouds, which were equatorial disc of positive charge, polar domes of negative charge and both signed outflows. Thus, the choice of  $\bar{\tau}_{pr}$  and  $\bar{\tau}_{po}$  in present simulation does not affect the results. We checked that if the lower system charge solution without pair creation is chosen as a initial condition, then the same result was obtained qualitatively.

## 4.3 Structure of Outer Gap

We here discuss the structure of the outer gaps for our results. For the discussion, the structure of the electrostatic potential and the intensity of  $E_{\parallel}$  in the pair creating region should be realized for our active solutions, where we obtained the solution with the several rates of the pair creation in simulation. Note that in our simulation, the  $E_{cr}$  is taken to be large artificially compared with a parameter for emission of gamma-ray to reality, in other words, pair creation rate is underestimated. For the reason, the size of the pair creating region is expanded and therefore the geometry of the outer gaps is not revealed quantitatively from our simulation. Although the structure of the outer gaps which are demonstrated the lower rate of the pair creation have contained some fraction of artifact, the result implies how the transition of the magnetosphere from the active state to the quiet state is realized with time for the pulsar, that is the evolution of the magnetosphere with the abundance of the pair plasma, which decreases with age of the pulsar.

Another important point, we can suggest the possibility of coexistence for polar cap and outer gap by comparing with the deviation from the force-free magnetosphere. If a force-free condition are satisfied elsewhere, we give the co-rotational potential under dipole magnetic field assumption,

$$\phi_{co} = \frac{\Omega\mu \sin^2 \theta}{cr}. \quad (29)$$

Then, the non-corotational potential defined  $\phi_{nco} \equiv \phi - \phi_{co}$ . Fig. 9 shows the non-corotational potential with color map and pair creating region with contour for  $B_0$  model on the meridional plane. The pair creating region become dramatically small compared with initial state in our simulation but the intensity of the  $E_{\parallel}$  in steady state remains larger than  $E_{cr}$  in the countour. Eventually, the pair creating regions remained in the middle latitudes and just above the poles. We don't distinguish between the process of the pair creations in present simulation, which are photon-photon collision and magnetic pair creation, and therefore the rate of the pair creation is only proportional to the product of the intensity of the  $E_{\parallel}$  and the volume of the gap. Thus, the supply of the plasma generated in the polar pair creating region was trivial compared with the one from the outer gaps, that is, our simulation underestimated the effect of shielding by pair plasma with magnetic pair creation in the polar cap. As Takata, Wang, & Cheng (2010) suggested that a new outer gap closure mechanism by the magnetic pair creation near the stellar surface is significant to realize the observed features of the gamma-ray pulsars, the effect of the different type of the pair creation should be investigated in future work.

In Fig. 9, the equatorial disc and polar domes has domain in which  $\phi_{nco}$  have deviation less than  $0.01\phi_{eff}$ . They are not accelerating region of the particle; dead zone. For our result, the existence of the dead zone provides a inspiration. Usually conventional polar cap and outer gap are defined on the last closed field line for GJ model and the poloidal current in the gaps directs oppositely, and therefore the gaps can not coexist. In present result, the dead zone in equatorial disc is reduced

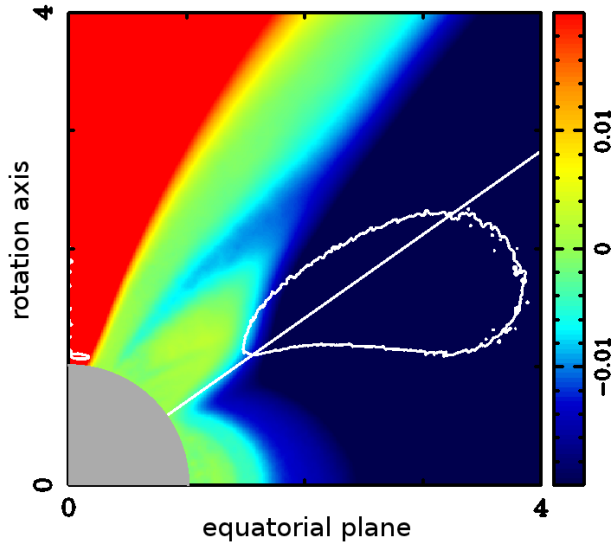


**Figure 9.** Distribution of non-corotational potential on meridional plane, and contour indicates isoline with  $E_{\parallel} = E_c$ . The color of map is normalized by 2% of the open field line voltage  $\phi_{\text{eff}}$ . The line in the middle latitude is null surface.

in the light cylinder and the effective last closed line is migrated to higher colatitude and the one in polar dome cut down the radius of the cone in which particle outflows. Note that the dead zones divide the last closed field line and would be able to coexist polar cap and outer gap on different magnetic surfaces. The poloidal current travels into the polar region of the stellar surface of the lower colatitude side of the polar dead zone, migrates to the magnetic surface with higher colatitude, and passes through the outer gaps. The current makes poloidal circulation beyond the light cylinder. Because we do not demonstrate detailed processes of pair creation and do not simulate with enough accuracy to resolve the size of the polar caps in present results and therefore it is not clear whether current from the polar cap is necessary condition or not. This interesting result should be discussed in future work.

For confinement for the robustness of our gap-wind solution, we carried out the models of some rates of the pair creation. We checked that  $E_{\parallel}$  in the gap saturates with a constant value for all steady states. Fig. 10 shows the saturated intensities of  $E_{\parallel}$  on the null surface in all simulations. All results had regions whose  $E_{\parallel}$  was larger than  $E_{\text{cr}}$  on the null surface. The width of the base of the bell-curve on the line with  $E_{\parallel}/E_{\text{cr}} = 1$  indicates typical size of the pair creating region on null surface. There is a tendency for the higher pair creation rate model ( $A_0 \rightarrow A_1 \rightarrow A_2 \rightarrow A_3$ ), which is parameterized by the frequency of the pair creation  $\bar{t}_{\text{pr}}$ , to decrease the size of the pair creating region and the intensity of  $E_{\parallel}$ . The saturated intensities are maintained just above the  $E_{\text{cr}}$ . When  $E_{\text{cr}}$  is taken to be much smaller value ( $A_0 \rightarrow A_4 \rightarrow A_5$ ), the pair creating region decreased in the same way and the saturated electric field intensity was held just higher than  $E_{\text{cr}}$ . In the lower  $E_{\text{cr}}$  model, the particles tended to screen out the gaps near the star although the outer edge of the pair creating region does not change. This indicates that the inner boundary of the outer gap, which has beak-like shape on the meridional plane, would not be connected to the star if we could carry out a much lower  $E_{\text{cr}}$  model. Considering from figure 7, the inner edge of the outer gap would be refined just outside the outer edge of the dead zone which is roughly defined as a magnetic field line footed on the stellar surface with  $32^\circ$  in our simulation. The inner boundary is slightly inside compared with that of the conventional outer gap model on the null surface. This agrees with Takata, Shibata, & Hirovani (2004) which is calculated the electrodynamics of an outer gap on the meridional plane with assumed external current, then as the current density increases, the inner boundary of the outer gap shifts toward the stellar surface. As previously explained, the main path of equatorial outflow exists outside of the dead zone, outer gap structure in our simulation can be maintained steadily.

We emphasize that the thickness of the pair creating region transversing the dipole magnetic surface would be related to the size of the region in which leakage of the disc particles takes place ( $\sim fR_l$ ) because the field aligned potential drop in the outer gap controls the super-rotation of the disc. Phenomenologically-postulated, the thickness of the outer gaps for old pulsars are shown by Zhang & Cheng (1997) in which they pointed out the effect of the finite mean free path of the gamma-ray for pair creation is important for defining the thickness of outer gap. In addition to this, the direction of the gamma-ray would be important to define the geometry of the outer gap because the particle has fast azimuthal motion in the gaps near the light cylinder, and therefore the gamma-ray is emitted to the azimuthal direction and the path of the gamma-ray should be considered with three dimensional geometry. We should consider the mean free path of gamma-ray for pair creation with a three-dimensional model in future work.

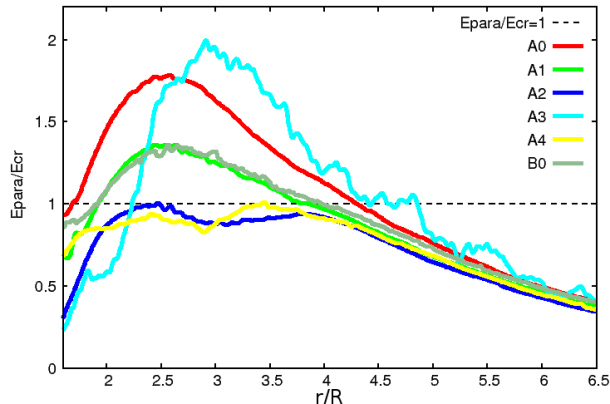


**Figure 10.** The curves are  $E_{\parallel}$  normalized by  $E_{cr}$  on the null surface. The horizontal axis indicates distance normalized by the stellar radius along the null surface. The tags indicate type of simulation referred in Table 1.

#### 4.4 Polar Gap

The polar cap accelerator has been an outstanding issue in the context of how one can understand radio emissions. We find a potential drop just above the stellar surface in our simulation in a similar fashion to the WS. The mechanism is very simple: in a steady state the negative charges created in the outer gap flow back to the star, and therefore the equal amount of negative charges should be emitted for steadiness. Then, the potential drop in the polar region of the stellar surface controls the polar flow of negative particles, which is represented by

$$\phi(\mathbf{R}) = \frac{\mu\Omega}{cR} \left( \sin^2 \theta - \frac{2}{3} \right) + \frac{Q_{\text{sys}}}{R} - \sum_{i=1}^n \frac{q_i}{R} \left( 1 - \frac{R}{r_i} \right). \quad (30)$$

In our all results of simulations,  $\phi_{\text{pole}}$  becomes slightly negative, and therefore the negative particles are pushed and easily escape to infinity. Implied by (30), this potential is kept by balance of the numbers of negative and positive particles in the magnetosphere (the second term) and  $Q_{\text{sys}}$  (the third term). Thus, we see that in the steady state  $Q_{\text{sys}}$  is determined so that the losses of negative and positive particles are balanced. This indicates that the polar caps have a close correlation to the injection of the electron from the the outer gaps. In the present case, the rate of the emitted particles from the polar region is less than would be capable of shielding the electric field above the pole, that is the current density from the pole is less than  $\rho_{GC}c$ , and therefore the unscreened potential increases gradually along polar magnetic field lines. In other words, this potential drop above the pole is not a conventional polar cap because the electric field is not shielded in finite distance near the stellar surface. There is a very interesting issue whether a potential drop near the polar region remains if enough electrons return from the outer gaps and are re-emitted from the pole or generated in the polar cap and then the emitted particles should form the space charge limited flow (Arons & Scharlemann 1979), but our simulation particle has large inertia length with 3% of stellar radius, and therefore the detailed structure might not be demonstrated. Note that our simulation contains the artificial polar gap arising from the intermittent emission of particle on the stellar surface, which is in the range of  $t_{\text{po}}c = 0.1R$  at a maximum. Unfortunately, it is difficult to take a much smaller value of  $t_{\text{po}}$  in the present parameter setting. Thus, it is not clear that polar electric field is shielded on the pole if pair creation process is considered in detail and whether the polar electric flow needs pair creation in polar cap or not. As shown by (Hirovani et al. 2003), the current from polar cap have a significant effect on outer gap electrodynamics, to discuss the possibility of existence of the polar caps linked with the outer gaps, the combination of localized simulation and global simulation would be needed.

## 5 CONCLUSION

For an axisymmetric pulsar magnetosphere, pair creation in the outer gaps results in expansion of rotating electrosphere and the trans-field drift motion due to radiation drag force near and beyond the light cylinder. Eventually, a steady state is achieved with the outflow of both particle species and global current loop on the meridional plane. We confirmed the pair starved static electrosphere shifts to the steady structure by the pair plasma in the gaps. The pair creation plays important role of metamorphosing from the static electrosphere to the steady structure nevertheless the pair creation rate is artificially suppressed in our present model. For more detailed discussion of the structure of the magnetosphere, the consideration of the mean free path of the pair creation, which is important for old pulsars having thick outer gaps, is needed to discuss the structure of the gap quantitatively. Additionally, a higher pair creation rate case should be simulated, then modification of the magnetic field from the dipolar changes the pattern of the outflow of the plasma and the structure of the gaps. Thus, our model can be developed to consider pulsar magnetosphere including much more pair plasma in the next paper.

## ACKNOWLEDGEMENTS

We would like to thank Jumpei Takata, Hiroyuki Takahashi, Syota Kisaka and anonymous referee for discussions and many helpful comments on the manuscript. Numerical simulations were carried out on the MUV system at Center for Computational Astrophysics, National Astronomical Observatory Japan.

## REFERENCES

- Abdo A. A. et al., *Science*, 325, 840  
Abdo A. A. et al., 2009b, *Science*, 325, 848  
Abdo A. A. et al., 2010, *ApJS*, 187, 460  
Abdo A. A. et al., 2009c, *ApJ*, 696, 1084  
Aliu E. et al, MAGIC Collaboration, 2008, *Science*, 322, 1221  
Arons J., Scharlemann E. T., 1979, *ApJ*, 231, 854  
Becker W., Trümper J., 1997, *A&A*, 326, 682  
Bucciantini N. et al., 2006, *MNRAS*, 368, 1717  
Cheng K. S., Ho C., Ruderman M., 1986a, *ApJ*, 300, 500  
—, 1986b, *ApJ*, 300, 522  
Daugherty J. K., Harding A. K., 1996, *ApJ*, 458, 278  
de Jager O. C., Djannati-Ataï A., 2008, *ArXiv e-prints*, 803  
Goldreich P., Julian W. H., 1969, *ApJ*, 157, 869  
Harding A. K., Muslimov A. G., 2002, *ApJ*, 568, 862  
Hirota K., Harding A. K., Shibata S., 2003, *ApJ*, 591, 334  
Hirota K., Shibata S., 1999, *MNRAS*, 308, 54  
Hobbs G. et al., 2004, *MNRAS*, 352, 1439  
Holloway N. J., 1973, *Nature*, 246, 6  
Jackson E. A., 1976, *ApJ*, 206, 831  
Kargaltsev O., Pavlov G. G., 2008, in *American Institute of Physics Conference Series*, Vol. 983, American Institute of Physics Conference Series, pp. 171–185  
Kennel C. F., Coroniti F. V., 1984a, *ApJ*, 283, 694  
—, 1984b, *ApJ*, 283, 710  
Kirk J. G., Skjæraasen O., Gallant Y. A., 2002, *A&A*, 388, L29  
Komissarov S. S., 2006, *MNRAS*, 367, 19  
Krause-Polstorff J., Michel F. C., 1985a, *MNRAS*, 213, 43P  
—, 1985b, *A&A*, 144, 72  
Makino J., Hiraki K., Inaba M., 2007, in *Proceedings of the 2007 ACM/IEEE conference on Supercomputing-Volume 00*, ACM, pp. 1–11  
McKinney J. C., 2006a, *MNRAS*, 367, 1797  
—, 2006b, *MNRAS*, 368, L30  
Michel F. C., 2004, *Advances in Space Research*, 33, 542  
Michel F. C., Smith I. A., 2001, in *Revista Mexicana de Astronomia y Astrofisica Conference Series*, Vol. 10, *Revista Mexicana de Astronomia y Astrofisica Conference Series*, J. Cantó & L. F. Rodríguez, ed., pp. 168–175  
Muslimov A. G., Harding A. K., 2003, *ApJ*, 588, 430  
—, 2004, *ApJ*, 606, 1143  
Nel H. I. et al., 1996, *ApJ*, 465, 898  
Pétri J., 2007, *A&A*, 469, 843  
Pétri J., Heyvaerts J., Bonazzola S., 2002a, *A&A*, 387, 520  
—, 2002b, *A&A*, 384, 414  
Possenti A., Cerutti R., Colpi M., Mereghetti S., 2002, *A&A*, 387, 993  
Rees M. J., Gunn J. E., 1974, *MNRAS*, 167, 1  
Romani R. W., 1996, *ApJ*, 470, 469  
Ruderman M. A., Sutherland P. G., 1975, *ApJ*, 196, 51  
Rylov I. A., 1977, *Ap&SS*, 51, 59  
Smith I. A., Michel F. C., Thacker P. D., 2001, *MNRAS*, 322, 209  
Spitkovsky A., 2004, in *IAU Symposium*, Vol. 218, *Young Neutron Stars and Their Environments*, F. Camilo & B. M. Gaensler, ed., pp. 357–+  
Takata J., Shibata S., Hirota K., 2004, *MNRAS*, 354, 1120

- Takata J., Shibata S., Hirotsu K., Chang H.-K., 2006, MNRAS, 366, 1310  
Takata J., Wang Y., Cheng K. S., 2010, ApJ, 715, 1318  
Uzdensky D. A., 2003, ApJ, 598, 446  
Wada T., Shibata S., 2007, MNRAS, 376, 1460  
Zhang B., Harding A. K., 2000, ApJ, 532, 1150  
Zhang L., Cheng K. S., 1997, ApJ, 487, 370

